REPORT DOCUMENTATION PAGE

1. REPORT DATE (DD-MM-YYYY)	2. REPORT TYPE	3. DATES COVERED (From - To)
15-02-2006	Final Technical Report	15-02-2005 - 30-11-2005

4. TITLE AND SUBTITLE

Studies of enhanced performance of the Mileura Widefield Array for solar observations and space weather

5a. CONTRACT NUMBER

5b. GRANT NUMBER

FA9550-05-1-0247

5c. PROGRAM ELEMENT NUMBER

6. AUTHOR(S)

Joseph E. Salah
D. Oberoi, C. Lonsdale R. Cannallo

5d. PROJECT NUMBER

5e. TASK NUMBER

5f. WORK UNIT NUMBER

7. PERFORMING ORGANIZATION NAME(S) AND ADDRESS(ES)

Massachusetts Institute of Technology Haystack Observatory
77 Massachusetts Avenue
Cambridge, MA 02139

8. PERFORMING ORGANIZATION REPORT NUMBER

9. SPONSORING/MONITORING AGENCY NAME(S) AND ADDRESS(ES)

USAF/AFRL/AFOSR
875 N. Randolph St., Room 3112
Arlington, MA 02139

10. SPONSOR/MONITOR'S ACRONYM(S)

11. SPONSOR/MONITOR'S REPORT NUMBER(S)

AFRL-SR-AR-TR-06-0263

12. DISTRIBUTION/AVAILABILITY STATEMENT

Approved for public release; distribution is unlimited

13. SUPPLEMENTARY NOTES

14. ABSTRACT

. The purpose of the study was to investigate developments that would enhance the capabilities of the Mileura Widefield Array-Low Frequency Demonstrator (MWA-LFD) for solar and space weather measurements. Enhancement of the angular resolution of the MWA-LFD to observe Type II Solar Radio Bursts was determined to be the best option, and can be accomplished by increasing the physical diameter of the array by a factor of -3. Key elements of the augmentation involve addition of 16 antenna clusters in two semi-circular rings of 3 and 4.5 km diameter, and expansion of the array correlator to accommodate the reduced from 3.4 to 1.13 arc minutes, and the collecting area is increased by 12%. The addition GPS receivers is also recommended to provide calibration of the Earth's ionosphere for heliospheric Faraday rotation measurements. Results from the early deployment of three antenna tiles at the Mileura station in West Australia are presented giving early indication of the excellence of the site environment and the capability of the instrument for solar observations.

15. SUBJECT TERMS

Low frequency radio array, space weather, heliosphere, solar radio bursts.

16. SECURITY CLASSIFICATION OF:			17. LIMITATION OF ABSTRACT	18. NUMBER OF PAGES	19a. NAME OF RESPONSIBLE PERSON
a. REPORT	b. ABSTRACT	c. THIS PAGE			Joseph E. Salah
Uncalssified	Unclassified	Unclassified		13	19b. TELEPHONE NUMBER (Include area code) 781-981-5400

Title: Studies of enhanced performance of the Mileura Widefield Array for solar observations
and space weather
Principal Investigator: Joseph E. Salah (MIT Haystack Observatory)
Collaborators: Divya Oberoi, Colin J. Lonsdale and Roger C. Cappallo (all at MIT/Haystack)

1. Background/Introduction

The purpose of the study was to investigate developments that would enhance the capabilities of
the Mileura Widefield Array-Low Frequency Demonstrator (MWA-LFD) for solar and space
weather measurements. The enhancement options included improvements of the MWA-LFD to
observe Type II solar radio bursts and locate them on the solar surface, examination of the array
design configuration to provide enhanced spatial resolution using distributed stations,
consideration of the expansion of the digital signal processor to accommodate an increase in the
number of beams from 16 to 32 or 64, and investigation of the use of GPS receivers within the
array for absolute calibration of the Earth's ionosphere to improve the accuracy of solar Faraday
rotation measurements.

As the study evolved, the proposal to enhance the MWA-LFD to enable scattering limited
observations of type II and other solar bursts was determined to be the most attractive option. As
a result, a DURIP proposal detailing this option was prepared and submitted to AFOSR.

In the following, we first summarize the rationale for our conclusion stated above, by presenting
the science motivation for observations of type II solar bursts and the details of the proposed
augmentation. The explorations of the other augmentation options are briefly summarized and
some solar observations conducted during the early deployment prototype testing activity of the
MWA-LFD are highlighted since part of the grant support was used for the analysis of data from
the Early Deployment experiments at Mileura. Several conference presentations were made
using the AFOSR support including the SHINE workshop (July 2005), the SPIE Space Weather
Instrumentation Conference (Aug 2005), the URSI General Assembly (Oct 2005), and the AGU
meeting (Dec 2005). These are listed in Section 8 of this report. The work will also be included
in a journal article currently in preparation.

2. Enhancement of the capabilities of the MWA-LFD to observe solar bursts

Solar radio bursts are manifestations of macroscopic release of energy in CMEs, solar flares and
other evolving magnetic structures. They are believed to be caused by shocks and energetic
electrons moving through the solar corona into the interplanetary medium. Much effort has been
invested in observing, cataloging and understanding the characteristics of these bursts since their
first detection in the early 1940s. This has lead to considerable progress in understanding of the
subject and an extensive body of literature as illustrated in the recent reviews by Bastian et al.
(1998), Robinson and Cairns (2000), Cairns and Kaiser (2002) and Gopalswamy (2004). Here we
focus on investigations of type II solar bursts.

2.1 The relationship between type II Solar bursts and CMEs

Type II bursts are often grouped into metric (m), decametric/hectometric (DH) and kilometric
(km), depending on the wavelength regime in which they are observed. While it is generally

accepted that DH and km type IIs are caused by CME driven shocks (Sheeley et al., 1985), the nature of energy source for the m-type II bursts is still controversial (see Gopalswamy et al., 1998; Cliver et al., 1999; Cairns and Kaiser, 2002 for recent reviews).

While all m-type II bursts seem to be associated with flares, only a few of the flares are associated with m-type II bursts. Similarly m-type II bursts have a very strong association with CMEs, though the converse is not true. There are reasons to believe that type II bursts are associated with *fast* CMEs (Gopalswamy et al., 1997, 1999; Cliver et al., 1999; Klien 1999). The qualifier *fast* implies that the CME should be traveling fast enough to drive a shock, i.e. its speed should exceed the fast mode speed in the ambient medium (Gopalswamy, 2004). The proponents of this argument explain the lack of a perfect correlation between m-type IIs and CMEs by pointing out that some CMEs may escape detection by the available instrumentation (Cliver et al., 1999). The skeptics, on the other hand, argue that some of the flares for which corresponding CMEs could not be located have been so bright (class X4) that the corresponding CMEs, had they existed, would be significantly above the detection threshold of instruments like the LASCO coronagraph even if they were to be directed diametrically away from the Earth. For the few cases where positional information is available for type II bursts, the radio source seems to occur well behind the leading edge of the CME (Wagner and MacQueen, 1983; Gary et al., 1984; Robinson and Stewart, 1985). This runs contrary to the idea of CME driven shocks, unless the emission originates only from the flanks of a CME driven shock. The competing scenario for energizing m-type IIs is using flare blast waves, i.e. they are caused by sudden heating of the coronal loops during flares. While it is consistent with the short life times of the bursts (Bougeret, 1985; Vrsnak, 1995; Gopalswamy et al., 1998) the primary difficulty with this model is that it does not produce any observable signature other than the m-type II burst itself.

While there is no consensus on the energy source of m-type II bursts, there is little disagreement that they are strongly correlated with the CMEs with the highest kinetic energy, the ones with the largest impacts on space weather and the near Earth environment. Metric type II bursts are associated with solar energetic particle (SEP) events. Imaging m-type II bursts will provide much needed new observational inputs and help resolve their insufficiently understood relationship with flares and CMEs.

2.2 Lack of suitable instrumentation for imaging.

Since the closure of Culgoora and Clark Lake observatories more than 20 years ago, radio images of burst emission have not been available. The 150-450 MHz frequency coverage of the Nançay Radio Heliograph in France (http://www.obs-nancay.fr/a_index.htm) has a poor overlap with the m-type II spectral regime which usually lies below 150 MHz. The Gauribidanur Radio Heliograph in India offers the right frequency coverage (40-150 MHz) but is a transit array limited in frequency agility, bandwidth (1 MHz) and baseline lengths (1.28 km East-West and 0.44 km North-South) (Ramesh et al., 1998) and is not efficient at imaging m-type II bursts which typically last for 5 to 15 min and have a frequency drift rate of around -0.16+/-0.11 MHz/sec (Mann et al., 1996). The Very Large Array (VLA) has an observing band at 74 MHz, but the 74 MHz dipoles are mounted on the dishes only for a few weeks a year. The Giant Meterwave Radio Telescope (GMRT) has an observing band at 150 MHz, but does not have the necessary frequency agility to respond to external triggers within a few minutes. These factors in combination with the infrequent and unpredictable nature of the type II bursts make it impractical to use these instruments for observing m-type II bursts. All investigations of solar burst emission currently rely solely on their dynamic spectra (frequency-time plots of intensities). While the available dynamic spectra span an impressive range of frequencies from as low as few MHz (Brunei Island Radio Spectrometer, Tasmania) to many GHz (Nobeyama Radio Heliograph, Japan) and provide adequate time and frequency resolution, they provide no information whatsoever about the location or morphology of the burst emission. If imaging observations could

be brought to bear on this problem, progress can be made on many of the currently open questions. For instance, the relative locations of the burst emission and the CME front will help in clarifying the relationship between radio bursts, CMEs, flares and magnetic reconnection. The observed angular size of the emission and its variation with frequency will provide information about source structure and scattering properties in the inner corona.

2.3 Estimating baseline requirements for scattering limited solar burst imaging

In the frequency range of interest to us, scatter broadening due to the solar corona is expected to be proportional to λ, the wavelength of observation[1] (and not λ^2), and this theoretical expectation matches observations (Suzuki and Dulk, 1985). Very few imaging observations exist for type II bursts, but due to their much higher frequency of occurrence, imaging studies of type III bursts have been more numerous. Type III bursts are believed to arise due to energetic electrons traveling on open magnetic field lines, leading to coherent plasma emission at the local plasma frequency. This scenario implies that the source region must be very compact and their observed sizes thus represent essentially a scatter broadened point source. Hence we use the observed properties of type III bursts to estimate the scatter broadening in the inner corona and to guide our estimates of baseline length required for scattering-limited imaging. Studies of time evolution of type III bursts at Culgoora often found that the smallest observed size was close to the resolution limits of its 3 km baselines (Stewart, 1974). It is therefore reasonable to assume that a 3 km baseline is not always sufficient for scattering-limited imaging. The current baseline design of the MWA-LFD provides longest baselines of 1.5 km and will hence need to be augmented, preferably beyond 3 km, in order to provide scattering size limited observations of solar bursts. We propose to extend the baseline lengths by a factor of 3 to ~4.5 km. We note that imaging of type III bursts also offers interesting science returns, as the type III emitting plasma flows along the open magnetic field lines, tracking its motion will map out the magnetic field geometry.

2.4 The MWA-LFD advantage

In view of the very low side-lobe levels in the point spread function (PSF) of the MWA-LFD, and the considerable advances in radio imaging algorithms, techniques and computing resources since the time solar bursts were last imaged, we expect the MWA-LFD to produce much higher fidelity and dynamic range images over narrow spectral widths (64 kHz) and rapid cadence (0.5 sec) providing an unprecedented tool for studying m-type II bursts. Taking advantage of the extremely intense burst radiation, we propose to use the observed phase variations to locate its position with the accuracy of a few arcseconds as it rises in the corona and drifts to lower frequencies. An independent measure of the coronal height at which the emission from a given frequency originates will allow us to determine the electron density at this height, rather than taking the usual route of using a coronal density model to map emission at a given frequency to a coronal height. In addition, being a much more sensitive instrument than the radio heliographs, the MWA-LFD will also explore any weaker spectral and/or temporal structures in solar burst emission, which are unobservable using current instrumentation.

3. Proposed augmentation

Based on the above studies, the principal goal of the proposed augmentation to the MWA-LFD array is to increase the physical diameter of the array by a factor of ~3, decreasing the solid angle subtended by the main peak of the point spread function by a factor of ~9, and sharply increasing

---

[1] We note that the λ dependence of the scattering size naturally implies that a given array size will provide scatter broadening limited observations for the entire frequency range.

the utility of the array for imaging and precisely locating solar burst emission. This goal can be accomplished by straightforward and cost-effective replication of hardware already developed for the main array, and appropriate deployment of the additional antenna systems to produce the necessary imaging characteristics. The key elements of the augmentation can be summarized as follows:

1. Addition of 16 antenna clusters in such a way as to achieve a high-quality point spread function with diameter 1/3 that of the original 1.5 km-diameter array. The nature of the science application requires that the monochromatic, instantaneous PSF be of high quality.

2. Expansion of the array correlator to accommodate the extra baselines due to the increase in the total number of antenna systems

3. Expansion of post-correlation computing capacity to accommodate the increased correlator output data rate due to the extra baselines

These changes will deliver the enhanced array resolution using existing hardware designs. The algorithmic and software capabilities that are required in order to utilize the enhanced hardware are either part of the existing array design, or are straightforward adaptations of existing techniques.

3.1 Sensitivity

The additional baselines must be sensitive enough that the high resolution portion of the array can detect the target phenomena in a time short compared to the expected evolution timescale of the bursts. During this time (a few seconds at most), the array must be readily calibratable, with particular reference to the ionosphere which can change swiftly, and which is capable of distorting and shifting solar burst images at a significant level.

Type II solar bursts exhibit flux densities in the range of 10^6 to 10^8 Jy, over a bandwidth of a few to 100 MHz. At this level, signal-to-noise ratio is not an issue for the array, or even for a single baseline in the array. The instrument will achieve an image SNR of at least 10^5 in 1 second and 8 kHz of bandwidth. A single baseline will deliver an SNR of order 200 in the same time and bandwidth, implying a phase measurement precision, on each of more than 10^5 baselines, of ~0.3 degree. Thus the important issue is not sensitivity, but is instead calibration and image quality. This is what has determined the scale of the augmentation, both in number and location of additional antennas.

3.2 Calibration

The calibration of low frequency arrays for high fidelity imaging is generally a challenging problem, for which we have devised an array design focused on maximizing the number of independent measurements of astronomical radio sources across the sky. We have also designed an array of very limited physical extent, so that all antennas have essentially similar views of the ionosphere, sharply reducing the number of parameters needed to calibrate the array. This results in a heavily over constrained calibration problem, and the expectation that a simple and efficient algorithm, based on measurements of purely refractive shifts in radio source positions, can be employed.

As the array physical extent is increased, the complexity of the required ionospheric calibration for accurate widefield imaging increases, in part because the assumption of purely refractive distortions of the sky starts to break down. However, for the solar burst application, the calibration problem is greatly simplified because the burst completely dominates the correlated

4

flux densities from the array. Under these circumstances, we are concerned only about the ionosphere in the direction of the burst, and the technique of conventional self-calibration as applied for decades in astronomical cm-wavelength arrays is fully adequate for high fidelity imaging. For our array, the technique must be adapted slightly to accommodate the MWA-LFD data flow architecture. This architecture involves application of slowly-varying antenna-based gain corrections in a predictive manner to the correlator output, followed by a gridding operation onto the *uv* plane. For the original, relatively compact array, conventional self-calibration is unnecessary, allowing us to sum multiple baselines into a single grid cell. Data from the longer baselines of the augmented array, which may benefit from self-calibration under ionospherically disturbed conditions at the lower frequencies, must instead be stored until selfcal solutions can be computed and applied. Computing the self-calibration solutions for the dominant burst source will be quick, and need involve only a subset of the 2,016 baselines formed by the 64 additional antenna tiles.

3.3 Configuration

The principal determinants of scientific utility for burst imaging will be the precision of imaging and source position determination on short timescales. These can best be maximized by designing for full *uv* coverage, and consequent high spatial dynamic range. Because of the high available SNR, the key requirement is *completeness* of coverage, rather than uniformity or smoothness of coverage, which can be achieved *post-facto* by data weighting. We must avoid array configurations that leave significant areas of the *uv* plane completely empty of measured visibilities. In practice, this sets a lower bound on the number of additional antennas required in order to achieve a given angular resolution enhancement.

The configuration design will make use of the fact that baselines between the core array of 500 tiles and a single outlier antenna will comprehensively fill a region of 1.5km extent in the *uv* plane. One obtains an "image" of the core array for each outlier antenna. Therefore, to comprehensively sample the plane out to an arbitrary radius, we can tile the plane by placing outlier antennas in a pattern so that their respective core array "images" overlap each other. Because of the reflection symmetry inherent in radio interferometer arrays, we need only do this for a range of position angles of 180 degrees as seen from the core array. We thus adopt two semicircular arcs of radius 1.8 and 3.0km, each populated with antenna clusters every 1.2 km or so, yielding 6 clusters on the inner semicircle, and 10 clusters on the outer semicircle. To maintain a roughly circular beam, the two semicircles will be on opposite sides of the core. Each cluster will consist of 4 antenna tiles plus a node enclosure, leading to a total of 64 additional tiles. The cluster diameter can be up to 250 meters. The use of 4 tiles per cluster instead of just one is for redundancy (in keeping with an overall instrument philosophy of fault-tolerance and low maintenance expense), to improve the *uv* coverage for the longest baselines, and to make more efficient use of node and communication infrastructure resources.

The currently proposed configuration is shown in Figure 1, with corresponding instantaneous monochromatic *uv* coverage. Outlier antennas, built as part of the proposed augmentation, are shown in red, and the original array configuration is shown in blue. In the *uv* coverage plot, core-core baselines are in blue, core-outlier baselines are in purple, and outlier-outlier baselines are in red. The blue, purple and red zones are what we refer to as zones 1, 2 and 3 respectively. The extent of zones 2 and 3 represent the increased angular resolution provided by the proposed augmentation. Zone 2 is very densely sampled, thanks to the 500 pre-existing core antennas. Zone 3 yields the highest resolutions but has somewhat sparser coverage. By virtue of the relatively large physical extent of the outlier clusters, however, this coverage is fairly uniform, and will be adequate for the burst imaging application. Stretching the array configuration along the N-S direction will be considered in order to compensate for the shortening of the projected baselines and maintain adequate resolution when observing the Sun at larger zenith distances.
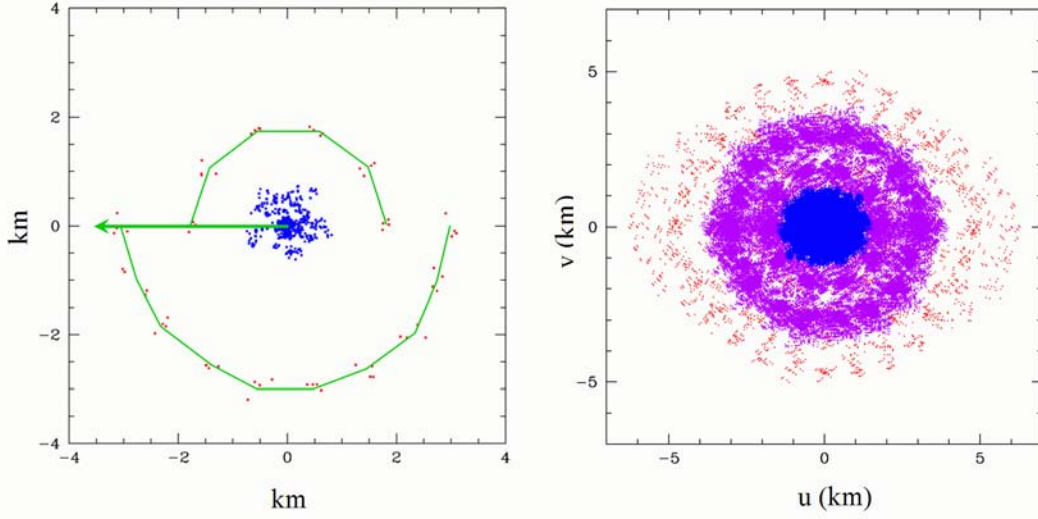
5

Figure 1. The left panel illustrates the layout for the proposed augmentation. The antennas in blue correspond to the core array and ones which form a part of the augmentation are shown in red. The thin green lines represent the cable and fiber trench layout for the remote stations and form a part of the augmentation. The thick green line represents the optical fiber to be provided by the OSI. The right panel shows the corresponding 'uv' coverage for source near zenith. The blue points correspond to the core-core baselines (zone 1), the purple ones to core-outlier baselines (zone 2) and the red ones to outlier-outlier baselines (zone 3).

Table 1 lists the subset of specifications of the array which are enhanced by the augmentation and provides a comparison of the core and augmented array at a glance.

Table 1. Specifications of the augmented array

	Core array	Augmented array
Number of receptors	8000 dual polarization dipoles	9024 dual polarization dipoles
Number of tiles (4x4 dipoles)	500	564
Effective collecting area[§]	~8000 m^2	~9024 m^2
Configuration	Centrally-condensed pseudo-random array ~1.5 km diameter	Core array + two semi circular rings of 3.0 and 4.5 km diameter.
Angular resolution[§]	3.4 arcmin	1.13 arcmin
Point source sensitivity[¶]	20 mJy in 1sec; 0.33 mJy in 1 hr	18 mJy in 1sec; 0.29 mJy in 1 hr
Number of baselines	124,750	158,766

[§] At 200 MHz   [¶] 32 MHz bandwidth at 200 MHz

3.4 System implications

3.4.1 Data transport

The data transport system for the outlier antenna clusters will be exactly the same as that for the main array. The central processing facility will be a few km distant, and fiber lighting requirements from the outlier clusters will be similar to those from the core clusters. The main issue is minimizing trenching and cabling costs for the outliers. This is most simply accomplished by the arrangement illustrated in figure 1, in which the green lines represent cable runs.

3.4.2 Correlation, and post-correlation data handling

We will retain the same correlator architecture for the augmented array as that already developed for the core array. In this system, sampled data are transformed to the frequency domain and filtered to high spectral resolution in the node enclosures in the field, before transmission to the central processing facility – this is the "F" part of the FX correlation. The cross-multiplication part of the system (the "X" part) is kept as simple as possible, by design, to facilitate the massively parallel processing of a very large number of baselines. There is no fringe rotation, as we use a coordinate system fixed at the zenith, and maintain a correlator time and frequency resolution fine enough to preserve the entire sky from horizon to horizon. The time and frequency resolution are adequate for a wide range of array applications, and are hardwired into the correlator (i.e. there is only one correlator "mode") for purposes of minimizing complexity and cost, both during development and operation.

The principal changes required to deal with the extra antennas and increased baseline lengths which characterize the proposed augmentation fall into two categories. First, the total number of antenna inputs, cross-multiplications, and accumulated visibility products will increase. We are proposing 64 additional antennas, so the input handling capacity of the correlation must increase by 12.5%, the cross-multiplication capacity must increase by 27%, and for a constant accumulation period, the output bandwidth must increase by 27%. All these increases will be handled by replication of correlator hardware, with relatively minor architectural impacts.

The second category of changes involves accommodation of the extra angular resolution. In order to maintain the full field of view, which is central to the array design and calibration strategy, it will be necessary to ensure that the output data has sufficient resolution in time and frequency. The existing design is based on 8 kHz frequency channels and 0.5 second time integration of correlation cross-products. These numbers are driven by astronomical science considerations, such as observations of narrow radio recombination lines, and compensating for dispersion across the band, and are more than adequate to satisfy the abovementioned field-of-view requirements. The major impact of the augmentation instead comes in the near-realtime post-correlation step of gridding and Fourier-inverting the visibilities, to form preliminary images which drive the calibration algorithms. The gridding step results in data compression, because multiple visibility samples typically fall into the same grid cell. In the augmented array, the increased angular resolution will require extension of the grid to proportionally larger uv distances, leading to about an order of magnitude increase in the grid size. Furthermore, the sparser coverage in the outer regions of the grid will reduce the mean data compression ratio achieved in gridding, and for a given spectral resolution will increase the data bandwidth in the post-gridding and calibration stages, beyond that due to the increase in the number of baselines.

However, the solar burst application does not require such high spectral resolution, and we propose to co-add 8 spectral channels into the outer region of the grid, for a resolution of 64 kHz in the high angular resolution data. We estimate that this will double the aggregate data rate in the instrument after the gridding step, with consequent augmentation requirements on post-gridding general computing resources, as noted in the budget

3.4.3 Observing program

To avoid contamination from the strong and variable solar emission, astronomical observations for the epoch of re-ionization and other projects requiring long integration times will usually be conducted at night. Large blocks of observing time will hence be available during the day for solar and heliospheric observations. During this demonstrator phase of the project, observations will be done in a campaign mode. For the duration of a campaign, the MWA-LFD will observe much like a dedicated solar facility. The observing time will be shared between different solar

7

and heliospheric applications, such as imaging of the sun and the bursts which require pointing at the Sun, and IPS and FR observations, which also involve pointing away from the Sun. Triggers for burst observations will come from the MWA-LFD itself and coordination with other nearby solar observatories, particularly with Learmonth, will be investigated. The solar and heliospheric data and analysis tasks will be shared with the project collaborators.

4. An increase in the number of beams for the IPS beamformer

The primary rationale to consider this option as part of our study was that an increase in the number of Interplanetary Scintillation (IPS) sources which could be simultaneously monitored would increase the number of constraints available for a tomographic reconstruction of the entire inner heliosphere. The present design allows for 16 beams and the augmentation was to consider increasing the number of beams to 32 or 64. The sensitivity of the array is sufficient to expect this number of IPS sources From an engineering perspective, a straight forward replication of currently planned beamformer hardware, accompanied by additional data routing hardware required to feed the signal to this hardware, can lead to an increase in the number of beams. However a factor of few increase in the number of beams would provide only an incremental improvement for the application of a technique which has already been demonstrated. While this enhancement does not pose much technical challenge and had little impact on the existing array design, we felt that returns from this will fall short of the expectations from a compelling DURIP proposal. It was therefore not pursued to the detail of developing an engineering design.

5. Remote stations to enable multi-station IPS

Another of the augmentation options studied was to add at least two remote stations to the proposed MWA-LFD in order to permit the array to do multi-station IPS, similar to what is currently done at the Solar Terrestrial Environment Laboratory (STELab) IPS array in Japan. In order to be able to measure solar wind velocity using multi-station IPS technique, the station separation needs to be of the order of the Fresnel radius or less. In the frequency range 200-300MHz, the higher part of the MWA-LFD band where IPS observations are most profitable, this corresponds to a distance of about 155 km to 190 km.

In order to be able to support multi-beaming, the remote stations need to have sufficient sensitivity to be able to observe comparatively fainter IPS sources. Figure 2 shows a plot of sensitivity as a function of number of MWA-LFD tiles. The blue symbol represents the sensitivity of the single station of the STELab remote antennas and requires 160 MWA-LFD tiles. The sensitivity of the STELab antennas limits them to observing about 40 sources per day.
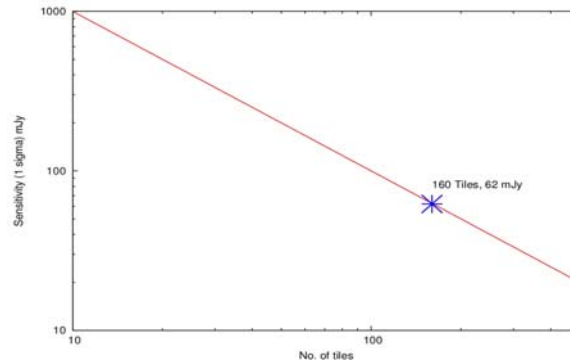

Figure 2. Number of MWA-LFD tiles needed (X axis) to achieve a given sensitivity (Y axis). Blue symbol mark the number of MWA-LFD tiles to equal the sensitivity of the existing STELab multi-station IPS system in Japan.

In order to go beyond what is being routinely done today, we would need to boost up the collecting area of the remote station sufficiently to allow it to do multi-beaming. Even if we want to match the performance of the existing STELab system, when one takes into account the additional cost of laying high bandwidth fiber to the remote stations, power generation for the remote stations, the additional antenna and beamformer hardware requirements, the project already grows way beyond the scope of a DURIP grant.

6. The use of GPS receivers for absolute calibration of the ionosphere

It is clear that a GPS dual-frequency receiver is needed to provide a measure of the background ionosphere to an accuracy of about 0.1% TEC. The array calibration system will provide the perturbation in electron density over the background ionosphere. A key location of the GPS receiver is in the center of the array core. Additional around the array will provide a variety of line-of-sight cuts into the ionospheric layer to improve the probability of a GPS satellite intersection with the array coverage. For example, a GPS receiver at Learmonth would be ideal, and perhaps receivers at Geraldton or Cue would be desirable. Thus a total of 3 or 4 receivers would fully provide the necessary measurements.

Measurements of TEC at distributed stations have been carried out by several groups. At the VLA, Erickson et al. (2001) used measurements from 4 GPS receivers with maximum separations of ~35 km to investigate ionospheric variations and to develop a simplified ionospheric model to compensate for these variations. The model was found to fit the data with a typical residual of 0.5 TEC unit, thus allowing compensation of Faraday rotation to better than 10 degrees at 327 MHz. A single GPS receiver at the center of the VLA could provide an indication of large scale fluctuations due to ionospheric structures larger than 1000 km. Small scale structures, less than 100 km, were difficult to compensate using the GPS grid unless the pierce point of the line-of-sight to the GPS satellite fell within the VLA's 4 degree isoplanatic patch.

At Millstone Hill Observatory, an experiment was conducted by Lincoln Laboratory in 1997-1998 using GPS receivers distributed across a 25 km baseline (Coster et al, 1998). Differences between the receivers were very small (~0.2 TEC units) during quiet conditions but were a factor of 10 greater during geomagnetic storms when TIDs were observed. The average deviation reported between two receivers was about 2 TEC units during such disturbed periods, with the largest value of 4 TEC units recorded during a Kp=9 event in May 1998.

Another study by Gao and Liu (2002) using 6 stations in Southern California distributed across 33 km baseline resulted in a recovery of ionospheric delays with a mean error of ~1.4% using 3D tomographic techniques, or ~0.5 TEC unit. Such recoveries are fully adequate for the calibration needs of the MWA-LFD deployment.

Regarding the type of receiver that is needed, the basic requirement is for a dual-frequency system to allow recover of the TEC. The Haystack atmospheric sciences group has specified GSV4004B receivers which are derived from the NovAtel EURO-3M GPStation-G2 card with a has high stability oscillator. The unit also contains some modified firmware by Van Dierendonck in Los Altos to allow TEC as well as scintillation measurement capability that would be useful for general ionospheric characterization at Mileura. Discussions with Dr. Keith Groves at AFRL have confirmed that his group is investigating various products and will be able to provide at least 3 GPS receivers for the Mileura application. AFRL also indicated that it has experience with linux-based realtime data collection from the GPS receivers that will also be contributed to our project.

7. The Early Deployment campaigns

In order to field-test the MWA-LFD prototype hardware, a series of observing campaigns were conducted at Mileura, Western Australia, between March - September 2005, each lasting about 2 weeks. The first of these campaigns started with a single tile in the field, another tile was added in each of the two successive campaigns and the last campaign was devoted to conducting science observations with the three tile interferometer. The tests involved researchers and students from MIT Haystack Observatory and the MIT Kavli Institute and from collaborating institutes in Australia, namely the Australian National University, University of Melbourne and Curtin University of Technology.

A first goal of the campaigns was to test the durability and performance of the dipole antennas and to make more precise measurements of the radio environment using the actual array elements. Figure 3 shows the first antenna test station deployed at Mileura in March 2005, consisting of 16 dual-polarization dipoles on a ground plane, and the analog beamformer powered by a battery-backed solar generator. The signals from the beamformer were transported ~150m via coax cable to an equipment van where they were converted to an 8 MHz IF, digitized, and stored on a PC for spectral analysis. A second antenna station was deployed in April 2005 and a third in June 2005, with baseline lengths of 145m, 211m and 325m between the three tiles.

Figure 3. The first completed antenna station with beamformer box and battery-backed solar power supply.

Figure 4 demonstrates the remarkably clean RFI environment at Mileura obtained with the MWA-LFD test station. These deep integrations of 30-60 minutes at representative frequencies of 102, 131, 189 and 327 MHz exhibit rms noise more than 30 dB below the galactic background, yet even at this high sensitivity, large tracts of frequency space show no evidence whatsoever of detectable RFI. Further, most of the observed features exhibit low temporal occupancy. This bodes extremely well for future high sensitivity experiments, solar and heliospheric measurements and other scientific projects.

Interferometry tests between the tiles demonstrated the array's ability to perform precision measurements of a number of discrete unresolved sources on the sky, with accurate fringe rate determinations to isolate contributions from specific sky locations. Several observations were also made of the Sun, with the most extensive being a full interferometry run for 6.5 hours, alternating between 96 and 196 MHz. A series of small flares were recorded as shown in Figure 5. Many short-duration spikes are visible, and the two brightest ones are identified by NOAA monitoring data as low-intensity type-III sweep-frequency radio bursts. There is a smooth phase ramp generated by the changing delay geometry of the observation as the earth rotates. In almost all cases, deviations from this smooth phase ramp are correlated with the spikes. A potential interpretation of this observation is that the solar emission during the spikes has a positional centroid that is displaced from that during quiescent periods.
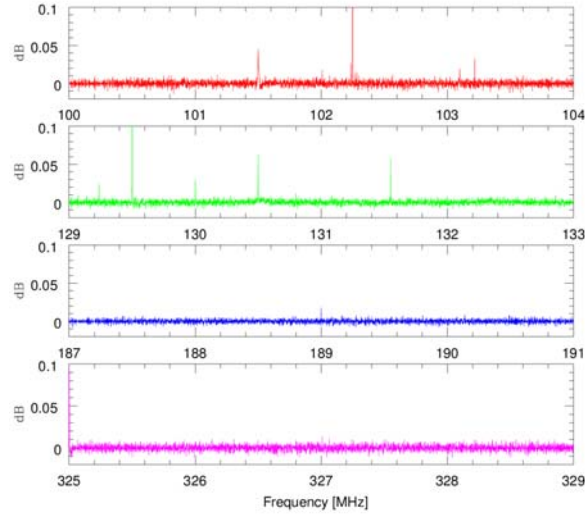
Figure 5. Deep integrations for 4 spectral windows of 4 MHz each, to characterize the low-level RFI environment at Mileura. Integration times at 102, 131, 189 and 327 MHz were 30, 60, 60 and 30 minutes respectively. The scales are in dB relative to the system noise, which is dominated by the sky background. These data have been median-filtered to remove the bandpass shape. Three of the displayed peaks are clipped on these plots; the peak at 102.25 MHz is ~1.5 dB, that at 129.5 MHz is ~1.7 dB, and the one at 325.0 MHz is ~0.16 dB. The resolution bandwidth is 1 kHz.
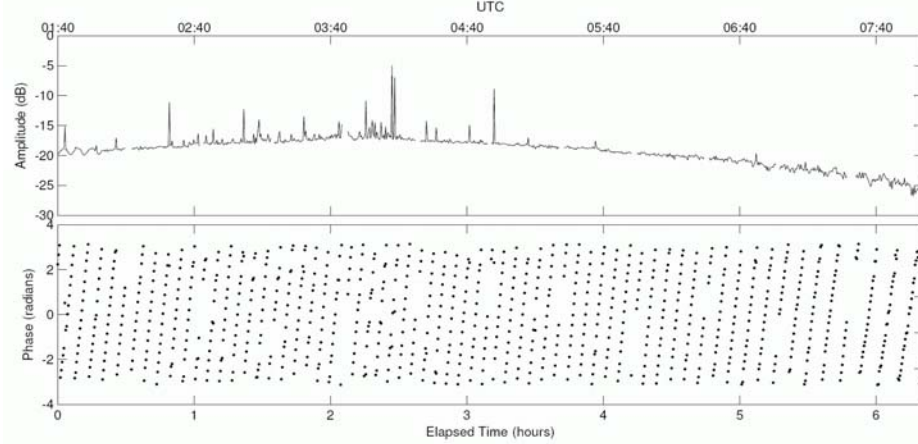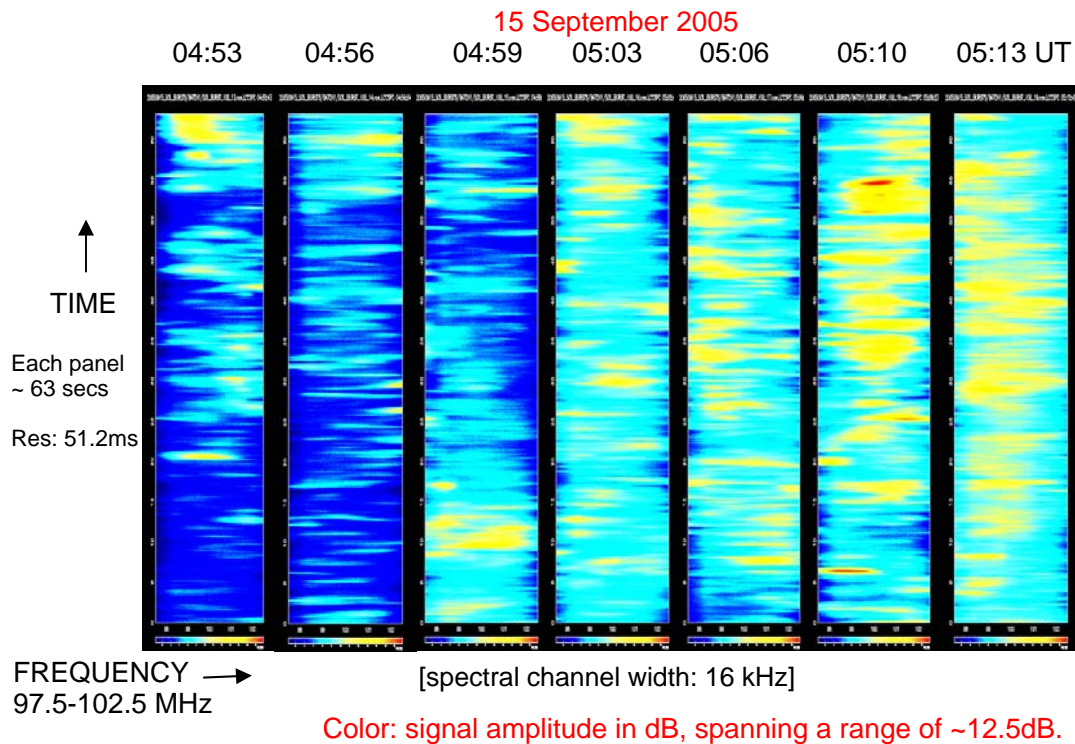

Figure 5. Correlated amplitude and phase at 96 MHz for the Sun over a 6.5 hour period on 27 April 2005. At this frequency and with a baseline of 145 m, one solar diameter corresponds to roughly three radians of interferometer phase.

Finally, in Figure 6, we present a result from the fourth early deployment campaign. The measurements of solar emission were obtained in the 97.5 - 102.5 MHz frequency band on one of the 3-tile interferometer baselines during a solar disturbance on 15 September 2005. Each of the panels represents ~63 s of data, with a data gap of ~140s between successive panels. The emission shown is on the same color scale of amplitude in dB and spans a range of ~12.5 dB. Frequency increases along the X axis and time along the Y axis. The fine details of burst emission shown in this figure are due to the excellent time resolution (51.2 msec) and spectral channel width (15.6 kHz) used in the observations. This level of emission usually remains below the detection threshold of most heliographs due to their coarser temporal and spectral resolution. Note the strong features at 5:10 UT which are sloping with frequency. Further analysis of phase data from the 15-16 September events is currently in progress and initial indications suggest the presence of a high velocity wave structure in the coronal region of magnetic reconnection.

15 September 2005

04:53   04:56   04:59   05:03   05:06   05:10   05:13 UT

TIME

Each panel ~ 63 secs

Res: 51.2ms

FREQUENCY →
97.5-102.5 MHz

[spectral channel width: 16 kHz]

Color: signal amplitude in dB, spanning a range of ~12.5dB.

At the time of these events, NOAA/SEC reports that type IV bursts were observed in the 25-180 MHz range throughout this period. Radio bursts at 8.8 GHz and 15.4 GHz were reported at 0459 UT and a C class X-Ray flare, accompanied by a radio flare, at 0500 UT.

8. Articles and presentations with AFOSR grant support:

Salah, J. E., C. J. Lonsdale, D. Oberoi, R. J. Cappallo, J. C. Kasper, "*Space Weather capabilities of low-frequency radio arrays*", Proceedings of the SPIE, vol 5901, in Solar Physics and Space Weather Instrumentation, S. Fineschi and R. Viereck, (ed), 5901G, 2005.

Oberoi, D., J. E. Salah, C. J. Lonsdale, R. J. Cappallo, and J. C. Kasper, "*Solar and heliospheric applications of low frequency radio arrays*" SHINE Workshop, Kona, Hawaii, July 2005.

Salah, J. E., C. J. Lonsdale, D. Oberoi, R. J. Cappallo, J. C. Kasper, "*Space Weather capabilities of low-frequency radio arrays*", SPIE Space Weather Instrumentation Conference, San Diego, CA, August 2005.

Oberoi, D., J. E. Salah, C. Lonsdale, J. C. Kasper, "*Potential of low-frequency radio arrays for solar and heliospheric observations",* URSI General Assembly, New Delhi, India, Oct 2005.

Salah, J. E, D. Oberoi, C. J. Lonsdale, Design progress and initial solar results from prototype tests of the Mileura Widefield Array, AGU Fall Annual Meeting, San Francisco, CA, Dec 2005.

REFERENCES

Bastian, T. S., Benz, A. O. and Gary, D. E., *Ann. Rev. of Astron. Astrophys.*, *36*, 131-188, 1998.

Bougeret, J.-L., *American Geophysical Union Geophysical Monograph Series*, *35*, 13-32, 1985.

Cairns, I. H. and Kaiser, M. L., In, *Review of Radio Science*, 1999-2992, Ross Stone, W. (Ed), IEEE Press, 749-774, 2002.

Cliver, E. W., Webb, D. F. and Howard, R. A., *Solar Phys. 187*, 89, 1999.

Coster, A. J., M. M. Pratt, B. P. Burke, and P. N. Misra, Characterization of atmospheric propagation errors for DGPS, Proceedings of ION 54th meeting, Denver, CO, June 1998.

Erickson, W. C., R. A. Perley, C. Flatters, and N. E. Kassim, Ionospheric corrections for VLA observations using local GPS data, *A&A*, 366, 1071-1080, 2001.

Gao, Y. and Z. Z. Liu, Precise ionospheric modeling using regional GPS network data, *J. Global Positioning Systems,* 1, 18-24, 2002.

Gary, D. E. et al., *Astron. Astrophys.*, *134*, 222, 1984.

Gopalswamy, N. et al., *Astrophys. J.*, *486*, 1086, 1997.

Gopalswamy, N. et al., *J. Geophys. Res.*, *103*, 307-316, 1998.

Gopalswamy, N. et al., *Astron. Astrophys.*, *347*, 684, 1999.

Gopalswamy, N., *Planetary and Space Science*, *52*, 1399-1413, 2004.

Klien, K.-L. et al., 1999, Astron. Astrophys., *346*, L53

Mann, G., Klassen, A., Classen, H.-T., Aurass, H., Scholz, D., MacDowall, R.J. and Stone, R.G., *Astron. Astrophys., 119,* 489-498, 1996.

Ramesh, R. et al., Solar Phys., *181*, 439-453, 1998.

Robinson, P. A. and Cairns, I. H., Radio Astronomy at Long Wavelengths In Stone, R. G., Weiler, K. W., Goldstein, M. L. and Bougeret, J.-L. (Eds), *Geophysical Mongraphs, 119*, AGU Press, 37-46, 2000.

Robinson, R. D. and and Stewart, R. T., *Solar Physics*, Vol. 97, 145-157, 1985.

Sheeley, N. R. et al., *J. Geophys. Res.*, 90, 163-175, 1985.

Stewart, R. T., *IAU Symp. 57: Coronal Disturbances*, 161, 1974.

Suzuki, S. and Dulk, G. A., *Solar Radiophysics*, 289-332, 1985.

Vrsnak, B., Ruzdjak, V., Zlobec, P. and Aurass, H., *Solar Phys.*, *158*, 331, 1995.

Wagner, W. J, and MacQueen, R. M., *Astron. Astrophys., 120*, 136, 1983.